A new polarization amplitude bias reduction method

Matias Vidal,[1,2]⋆ J. P. Leahy[1]⋆ and C. Dickinson[1]⋆

[1]*Jodrell Bank Centre for Astrophysics, Alan Turing Building, School of Physics and Astronomy, The University of Manchester, Oxford Road, Manchester M13 9PL, UK*

[2]*Departamento de Astronomía, Universidad de Chile, Casilla 36-D, Santiago, Chile*

ABSTRACT

Polarization amplitude estimation is affected by a positive noise bias, particularly important in regions with low signal-to-noise ratio (SNR). We present a new approach to correct for this bias in the case there is additional information about the polarization angle. We develop the 'known-angle estimator' that works in the special case when there is an independent and high SNR ($\gtrsim 2\sigma$) measurement of the polarization angle. It is derived for the general case where the uncertainties in the Q, U Stokes parameters are not symmetric. This estimator completely corrects for the polarization bias if the polarization angle is perfectly known. In the realistic case, where the angle template has uncertainties, a small residual bias remains, but that is shown to be much smaller that the one left by other classical estimators. We also test our method with more realistic data, using the noise properties of the three lower frequency maps of *Wilkinson Microwave Anisotropy Probe*. In this case, the known-angle estimator also produces better results than methods that do not include the angle information. This estimator is therefore useful in the case where the polarization angle is expected to be constant over different data sets with different SNR.

Key words: polarization – radiation mechanisms: non-thermal – methods: data analysis – methods: statistical – techniques: polarimetric.

1 INTRODUCTION

It has long been noticed that observations of linear polarization are subject to a positive bias (Serkowski 1958). Given the positive nature of the polarization amplitude, $P = \sqrt{Q^2 + U^2}$, even if the true Stokes parameters Q_0, U_0 are zero, P will yield a non-zero estimate in the presence of noise. The effect is particularly important in the low signal-to-noise ratio (SNR) regime. Ways to correct for the bias have been studied in detail for the special case where the uncertainties for (Q, U) are equal and normally distributed around their true value (Q_0, U_0) (Wardle & Kronberg 1974; Simmons & Stewart 1985; Vaillancourt 2006; Quinn 2012). Montier et al. (2015a,b) give a useful review comparing different bias reduction methods.

In this paper, we propose a new approach, useful when there is an independent measurement of the polarization angle $\chi = 0.5 \arctan(U/Q)$. This situation occurs, for instance, in the polarization data sets from Wilkinson Microwave Anisotropy Probe (*WMAP*; Bennett et al. 2013) and *Planck* (Planck Collaboration I 2014), where over a range of frequency the polarization angle is expected to be nearly constant (e.g. synchrotron radiation will have the same polarization angle at different frequencies as this angle depends on the direction of the magnetic field of the emitting medium), and the variation of the polarized intensity with frequency is of interest. Using simulations, we test the performance of this estimator compared to previous methods from the literature that do not include angle information. In Section 2, we show the origin of the bias and we describe some methods used to correct for it. In Section 3, we derive our new estimator, its uncertainty and residual bias. In Section 4, we use simulations to test its performance. Section 5 concludes.

2 BIAS CORRECTION METHODS

We will first review the simple case when the uncertainties in Q and U are equal, and then study the more general case with asymmetric uncertainties.

⋆E-mail: mvidal@das.uchile.cl (MV); j.p.leahy@manchester.ac.uk (JPL); clive.dickinson@manchester.ac.uk (CD)
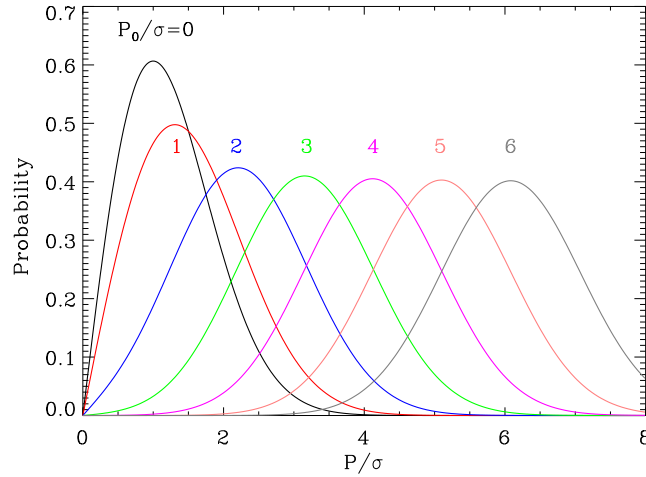
Figure 1. Rice distribution (equation 3) plotted for different values of the true SNR, P_0/σ. The asymmetry and bias are clear in the low SNR level. At high SNR, the distribution converges to a Gaussian with standard deviation σ centred at $\sqrt{P_0 + \sigma^2}$.

2.1 Symmetric uncertainties

Let us take (Q_0, U_0) as the true Stokes parameters from a source and (Q', U') the measured ones. We can write the joint probability distribution function (pdf) for (Q', U') as the product of the individual normal distributions

$$f(Q', U') = \frac{1}{2\pi\sigma^2} \exp\left[-\frac{(Q' - Q_0)^2 + (U' - U_0)^2}{2\sigma^2} \right],\tag{1}$$

where $\sigma_Q = \sigma_U = \sigma$ is the uncertainty in Q' and U'.

Transforming into polar coordinates using the definitions for the polarization amplitude $P = \sqrt{Q^2 + U^2}$ and the polarization angle $\chi = \frac{1}{2}\arctan(U/Q)$, we have

$$f(P', \chi') = \frac{P'}{\pi\sigma^2} e^{-[P'^2 + P_0^2 - 2(P'\cos 2\chi' P_0 \cos 2\chi_0 + P\sin 2\chi' P_0 \sin 2\chi_0)]/2\sigma^2} = \frac{P'}{\pi\sigma^2} e^{-(P'^2 + P_0^2)/2\sigma^2} e^{-P'P_0 \cos[2(\chi' - \chi_0)]/\sigma^2}.\tag{2}$$

The marginal probability distribution for P' is obtained by integrating $f(P', \chi')$ over χ'. This angular integral can be written as a function of the modified Bessel function of first type $I_0(z)$, yielding the Rice distribution for polarization (Rice 1945):

$$R(P'|P_0) = \frac{P'}{\sigma^2} I_0\left(\frac{P'P_0}{\sigma^2}\right) e^{-(P'^2 + P_0^2)/2\sigma^2}.\tag{3}$$

It is important to note that the integral of $R(P'|P_0)$ represents the probability of measuring P' inside an interval for a given true polarization P_0. Fig. 1 shows $R(P'|P_0)$ for different SNR. The bias, defined as $\langle P' \rangle - P_0$, arises because this probability distribution is not symmetric, and becomes clear in Fig. 1 at low SNR. Even when the true SNR is zero (black curve in the figure), the measured value is close to 1. At large SNR, the distribution approaches a Gaussian with mean close to P_0 and standard deviation close to σ.

Simmons & Stewart (1985) compared five estimators for P_0 (including the uncorrected P'), and concluded that the one with smallest residual bias when $P_0/\sigma \gtrsim 0.7$ is that suggested by Wardle & Kronberg (1974):

$$\left.\frac{\partial R}{\partial P'}(P', P_0)\right|_{P_0 = \hat{p}} = 0.\tag{4}$$

(note that this is not the maximum likelihood estimator). Even at moderate SNR, the rice distribution is not centred at the measured SNR, this can be seen in Fig. 1, where the distributions have mean $\sqrt{P_0 + \sigma^2}$. This motivated Wardle & Kronberg (1974) to propose a very simple estimator

$$\hat{p}_{AS} = \begin{cases} \sqrt{P'^2 - \sigma^2} & P' \geq \sigma; \\ 0 & \text{otherwise.} \end{cases}\tag{5}$$

This approximates equation (4), and also has the virtue of giving lower bias at very low SNR, albeit at the cost of a 1 per cent overcorrection near SNR = 2; this has been widely used in practice. Montier et al. (2015b) compared various estimators of the polarization angle in terms of the residual bias, risk, variance and Gaussianity. An unwanted property of the asymptotic (AS, equation 5) estimator is that the distribution of the estimator is discontinuous as it yields zeroes below a particular SNR (see equation 5). It is illuminating to re-write equation (5) in terms of the error in the polarization angle, $\sigma_\chi = \sigma/2P'$, so

$$\hat{p}_{AS} = P'\sqrt{1 - 4\sigma_\chi^2}.\tag{6}$$
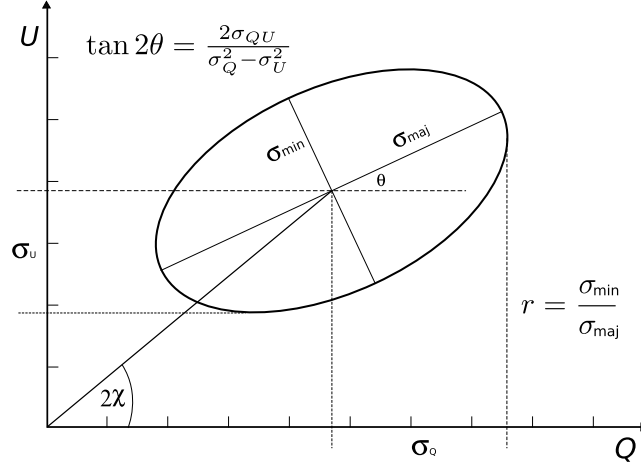
Figure 2. Error ellipse in the (Q, U) plane showing how the polarization angle χ and the rotation angle θ are related.

This emphasises that the source of the bias is the error in the angle of the (Q, U) vector, which contributes a component of the error vector orthogonal to the true polarization with length $P' \sin 2\Delta_\chi$, and is added in quadrature to the parallel component, hence always contributing a positive bias.

For the polarization angle, here we use the naive estimator, $\chi = \frac{1}{2} \arctan(U/Q)$, which is completely unbiased. The uncertainty of this estimator, on the AS case where $P_0 \gg \sigma$ is (Vinokur 1965; Montier et al. 2015a)

$$\sigma_\chi = \sqrt{Q'^2 \sigma_Q^2 + U'^2 \sigma_U^2}/2P^2. \tag{7}$$

2.2 Asymmetric uncertainties

The previous case in which the uncertainties in (Q', U') are equal and uncorrelated is well understood. The asymmetric case is interesting as many polarization data sets have this characteristic. For example, the cosmic microwave background experiments *WMAP* (Bennett et al. 2013) and *Planck* (Planck Collaboration I 2014) have correlations between the (Q', U') uncertainties due to non-uniform azimuthal coverage for each pixel in the sky. This case has been recently studied by Montier et al. (2015a,b) and Plaszczynski et al. (2014). The error distribution in these cases is an elliptical 2D Gaussian in (Q', U'), characterized by a covariance matrix (e.g. Kendal, Stuart & Ord 1994)

$$C = \begin{pmatrix} \sigma_Q^2 & \text{cov}_{QU} \\ \text{cov}_{QU} & \sigma_U^2 \end{pmatrix} \tag{8}$$

Defining a (Q, U) error vector

$$\boldsymbol{\delta} = \begin{pmatrix} Q' - Q_0 \\ U' - U_0 \end{pmatrix}, \tag{9}$$

we have

$$f(Q', U') = \frac{1}{2\pi\sqrt{\det[C]}} \exp\left[-\frac{\boldsymbol{\delta}^T C^{-1} \boldsymbol{\delta}}{2}\right]$$

$$= \frac{1}{2\pi\sigma_Q\sigma_U\sqrt{1-\rho^2}} \exp\left[-\frac{1}{2(1-\rho^2)}\left(\frac{(Q'-Q_0)^2}{\sigma_Q^2} + \frac{(U'-U_0)^2}{\sigma_U^2} - \frac{2\rho(Q'-Q_0)(U'-U_0)}{\sigma_Q\sigma_U}\right)\right], \tag{10}$$

where ρ is the correlation coefficient between (Q_0, U_0),

$$\rho = \frac{E[(Q'-Q_0)(U'-U_0)]}{\sigma_Q\sigma_U} = \frac{\text{cov}_{QU}}{\sigma_Q\sigma_U}. \tag{11}$$

The error ellipse in the Q, U plane will be rotated an angle θ in the case of a non-zero cov_{QU} (see Fig. 2). In terms of the components of the covariance matrix,

$$\theta = \frac{1}{2} \arctan \frac{2\text{cov}_{QU}}{\sigma_Q^2 - \sigma_U^2}. \tag{12}$$

The error ellipse has axial ratio

$$r = \frac{\sigma_{\text{min}}}{\sigma_{\text{maj}}}, \tag{13}$$

where

$$\sigma_{\text{maj}}^2 = \frac{1}{2}\left(\sigma_Q^2 + \sigma_U^2 + \sqrt{\left(\sigma_Q^2 - \sigma_U^2\right)^2 + 4\text{cov}_{\text{QU}}{}^2}\right) \tag{14}$$

$$\sigma_{\text{min}}^2 = \frac{1}{2}\left(\sigma_Q^2 + \sigma_U^2 - \sqrt{\left(\sigma_Q^2 - \sigma_U^2\right)^2 + 4\text{cov}_{\text{QU}}{}^2}\right). \tag{15}$$

Allowing for correlated variables, the error in any $f(Q', U')$ is to first order

$$\sigma_f^2 = \left(\frac{\partial f}{\partial Q'}\right)^2 \sigma_Q^2 + 2\frac{\partial f}{\partial Q'}\frac{\partial f}{\partial U'}\text{cov}_{\text{QU}} + \left(\frac{\partial \text{f}}{\partial \text{U}'}\right)^2 \sigma_{\text{U}}^2. \tag{16}$$

Hence (Montier et al. 2015a),

$$\sigma_P^2 = \frac{Q'^2\sigma_Q^2 + 2Q'U'\text{cov}_{\text{QU}} + U'^2\sigma_{\text{U}}^2}{P'^2} = \cos^2 2\chi'\,\sigma_Q^2 + 2\cos 2\chi'\sin 2\chi'\,\text{cov}_{\text{QU}} + \sin^2 2\chi'\,\sigma_U^2 \tag{17}$$

$$\sigma_\chi^2 = \frac{\sin^2 2\chi'\,\sigma_Q^2 - 2\cos 2\chi'\sin 2\chi'\,\text{cov}_{\text{QU}} + \cos^2 2\chi'\,\sigma_U^2}{4P'^2}, \tag{18}$$

When $r \neq 1$, the polarization bias depends on the polarization angle χ_0, more specifically on $\theta - 2\chi_0$, as well as on p_0. The AS estimator from equation (6), $\hat{p}_{\text{AS}} = P'\sqrt{1 - 4\sigma_\chi^2}$, still applies, provided we use the generalized form of σ_χ derived above. We note that equation (18) is derived in the small-error approximation and uses the observed polarization angle, χ', as a surrogate for the true polarization angle χ_0, which is unobjectionable in the high SNR regime. When SNR is low, it is not so obvious that this is appropriate, but we will verify by simulations that the estimator remains reasonably effective.

The preferred estimator of Montier et al. (2015b), is the 'modified asymptotic estimator', MAS (Plaszczynski et al. 2014), which using the above notation is given by

$$\hat{p}_{\text{MAS}} = P'\left[1 - 2\sigma_\chi^2\left(1 - e^{-P'^2/b^2}\right)\right], \tag{19}$$

3 KNOWN-ANGLE ESTIMATOR

As we will see, all estimators based exclusively on one observed (Q', U') measurement give a significant positive bias at very low SNR. However, this can be overcome if we have an independent estimate of the polarization angle χ. We will refer to this as the 'template' observation, in contrast to the 'target' observation to be de-biased.

We will build a new estimator, based on the maximum likelihood estimator, assuming that the true angle χ_0 is known. We will later calculate the residual bias which emerges because of uncertainty in our template angle, hereafter denoted χ, as distinct from the true angle χ_0 and the observed angle χ' from the target observation.

To find our known-angle estimator, $\hat{p}_\chi$, we take the joint pdf for the observed values (Q', U') with asymmetric uncertainties from equation (10). Since $Q_0 = P_0 \cos 2\chi_0$ and $U_0 = P_0 \sin 2\chi_0$,

$$f(Q', U') = \frac{1}{2\pi\sigma_Q\sigma_U\sqrt{1 - \rho^2}}\exp\left[-\frac{1}{2(1 - \rho^2)}\left(\frac{(Q' - P_0\cos 2\chi_0)^2}{\sigma_Q^2} + \frac{(U' - P_0\sin 2\chi_0)^2}{\sigma_U^2}\right.\right.$$
$$\left.\left. - \frac{2\rho(Q' - P_0\cos 2\chi_0)(U' - P_0\sin 2\chi_0)}{\sigma_Q\sigma_U}\right)\right]. \tag{20}$$

The maximum likelihood estimator in this case, $\hat{p}_\chi$, is defined by the condition:

$$\left.\frac{\partial f(Q', U')}{\partial P_0}\right|_{P_0 = \hat{p}_\chi} = 0. \tag{21}$$

With the assumption that $\chi_0 = \chi$, this leads to the expression for the de-biased polarization amplitude,

$$\hat{p}_\chi = \frac{\sigma_U^2 Q'\cos 2\chi - \text{cov}_{\text{QU}}(Q'\sin 2\chi + U'\cos 2\chi) + \sigma_Q^2 U'\sin 2\chi}{\sigma_U^2 \cos^2 2\chi - 2\text{cov}_{\text{QU}}\sin 2\chi\cos 2\chi + \sigma_Q^2\sin^2 2\chi}. \tag{22}$$

We note that if the observed polarization angle χ' is used as a surrogate for χ_0, then $\hat{p}_\chi = p' = \sqrt{Q'^2 + U'^2}$ and there is no correction whatsoever – we do need an independent constraint on χ to benefit from this approach.

The error in $\hat{p}_\chi$ is given via equation (16):

$$\sigma_{\hat{p}_\chi}^2 = \frac{\sigma_Q^2\sigma_U^2 - \sigma_{QU}^2}{\sigma_U^2 \cos^2 2\chi - 2\text{cov}_{\text{QU}}\sin 2\chi\cos 2\chi + \sigma_Q^2\sin^2 2\chi} = \frac{\det[C]}{4P'^2\sigma_\chi^2}. \tag{23}$$
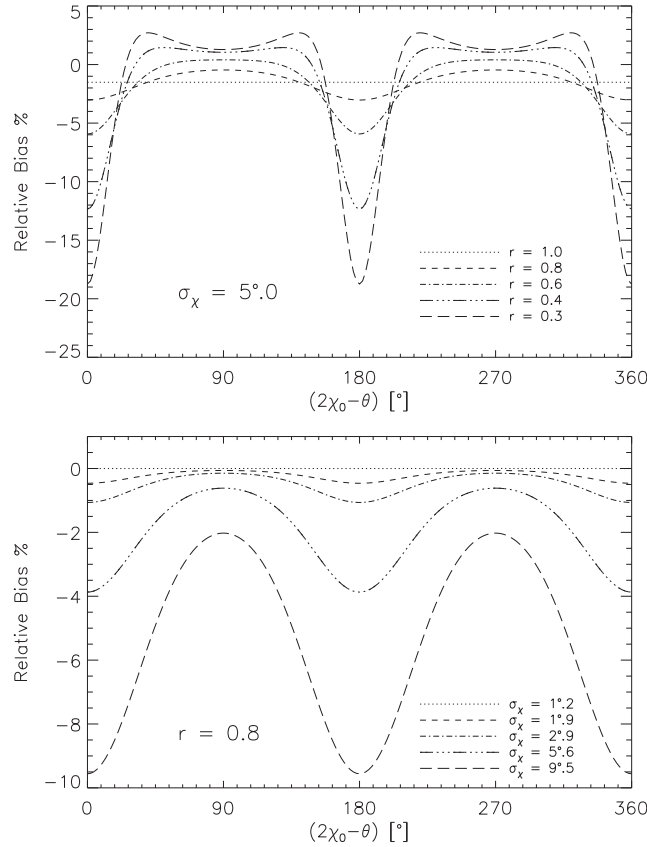
Figure 3. Fractional bias of the known-angle estimator, $\hat{p}_\chi$, for different values of the error ellipse ($r = \sigma'_U/\sigma'_Q$) and an uncertainty in the template angle of $5°$ (top). The bottom plot shows the residual fractional bias of $\hat{p}_\chi$ for different values of the uncertainty in the template angle, σ_χ, for a fixed value of $r = 0.8$. Both plots are calculated with $P_0 = 1$.

The known-angle estimator still contains a residual bias, due to the uncertainty in the template angle χ. Specifically, the expected value of the fractional bias is

$$b_\chi \equiv \frac{\langle \hat{p}_\chi \rangle - P_0}{P_0} = \int_\chi f(\chi|\chi_0) \int_{Q',U'} f(Q', U'|P_0, \chi_0) \frac{\hat{p}_\chi}{P_0} \, d\chi \, dQ \, dU - 1. \tag{24}$$

Since $\hat{p}_\chi$ is linear in $Q' = P_0 \cos 2\chi_0 + \delta_Q$ and in $U' = P_0 \sin 2\chi_0 + \delta_U$, integrating over the Gaussian probability distribution of (Q', U') eliminates the dependence on the deviations δ_Q, δ_U, and we have

$$b_\chi = \int_\chi f(\chi|\chi_0) \frac{\sigma_U^2 P_0 \cos 2\chi_0 \cos 2\chi - \text{cov}_{QU} P_0(\cos 2\chi_0 \sin 2\chi + \sin 2\chi_0 \cos 2\chi) + \sigma_Q^2 P_0 \sin 2\chi_0 \sin 2\chi}{P_0(\sigma_U^2 \cos^2 2\chi - 2\text{cov}_{QU} \cos 2\chi \sin 2\chi + \sigma_Q^2 \sin^2 2\chi)} \, d\chi - 1, \tag{25}$$

where $f(\chi|\chi_0)$ is the pdf of the template angle.

The amplitude of the polarized signal, P_0, cancels, so the residual bias just depends on the axial ratio of the (Q, U) error ellipse, r, and the difference between the orientation of the ellipse, θ, and that of the true (Q_0, U_0) vector, $2\chi_0$ (see Fig. 2). If the angle is known exactly so $f(\chi|\chi_0) = \delta(\chi - \chi_0)$, the residual bias vanishes.

In the special case where $\text{cov}_{QU} = 0$, so $r = \sigma_U/\sigma_Q$, we have

$$b_\chi = \int_\chi f(\chi|\chi_0) \frac{r^2 \cos 2\chi_0 \cos 2\chi + \sin 2\chi_0 \sin 2\chi}{r^2 \cos^2 2\chi + \sin^2 2\chi} \, d\chi - 1. \tag{26}$$

The top panel of Fig. 3 shows the bias for different axial ratios of the error ellipse as function of the polarization angle (see the angle definitions in Fig. 2). Here the uncertainty in the template angle is Gaussian (cf. equation 7) and it is fixed at $\sigma_\chi = 5°$. If the error distribution is symmetric ($r = 1$), the bias is constant (cf. equation 26). The bottom panel of Fig. 3 shows the bias for different values of the uncertainty in the template angle, for an error ellipse with axial ratio $r = 0.5$. The bias is usually negative, i.e. the polarized intensity is slightly underestimated.

When the template for the angle has an SNR at least 2 times larger than the target, the known-angle estimator thus gives excellent performance at very low signal-to-noise levels, where other estimators have large residual biases. However, for a given uncertainty in χ, the bias does not decrease as the signal in (Q', U') rises, unlike all the standard estimators. In practical use, the estimator is only worthwhile when a template observation with substantially higher SNR than the target observations is available; fortunately, this situation is fairly common, as discussed in Section 4.3.
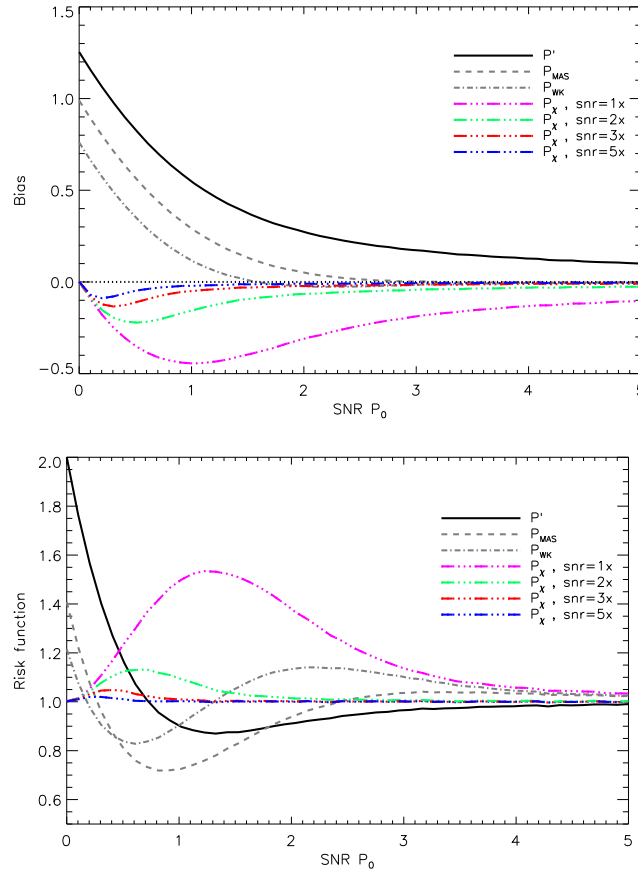
Figure 4. Residual bias (top) and risk function (bottom) for the naive, $\hat{p}'$ (continuum line), $\hat{p}_{MAS}$ (dashed), $\hat{p}_{AS}$ (dot–dashed line) and $\hat{p}_\chi$ (colours) estimators as a function of the SNR of the true polarization amplitude P_0. As the residual bias and risk function of the known-angle estimator depends on the uncertainty of the high SNR template, we show these two functions for four different values of the uncertainty of the high SNR template: same SNR of the target in magenta, 2 times the SNR of the target in green, 3 times in red and 5 times better in blue. Both plots are for the isotropic case, $\sigma_Q = \sigma_U$.

4 TESTS OF THE ESTIMATORS

Here we compare the effectiveness of three bias reduction methods using Monte Carlo simulations for a range of SNR. This is to show what can be gained when including additional angle information from a higher signal-to-noise template. In Section 4.2, we study the residual bias in a single pixel for a range of SNR in (Q, U). Section 4.3 tests the methods using real noise values from the *WMAP* polarization data.

Using Monte Carlo simulations, we measure the residual bias in a single pixel for four polarization amplitude estimators.

(i) $\hat{p}' = P' = \sqrt{Q'^2 + U'^2}$, the naive estimator with no correction for bias.
(ii) $\hat{p}_{MAS}$, the Plaszczynski et al. MAS estimator, from equation (19).
(iii) $\hat{p}_\chi$, the known-angle estimator, from equation (22).

4.1 Isotropic case

We ran 10^6 Gaussian noise realizations for the Q, U Stokes parameters. For the known-angle estimator, we also produced an additional set of 10^6 noise realizations for the high signal-to-noise template Q, U, which accounts for the uncertainty in the known angle. We start with the simpler case where σ_Q and σ_U are not correlated. We studied the bias, defined as bias $= \hat{p} - P_0$ and the risk function $= \langle (\hat{p} - P_0)^2 \rangle$, for the different estimators. In Fig. 4, we show on the top panel the residual bias of the estimators as a function of the observed $\text{SNR}_P \equiv P_0/\sigma_P$, with σ_P defined in equation (17). We show four lines for $\hat{p}_\chi$, which correspond to different values of the SNR of the angle template. The bottom panel of Fig. 4 shows the risk function for the different estimators.

We can see that the known-angle estimator performs very well in the case when the polarization angle is known with relatively high precision, i.e. when the SNR of the template is >2 to 3 times the SNR of the target.

The construction of the known-angle estimator allows for negative values of $\hat{p}_\chi$. Fig. 5 shows the distributions of $\hat{p}_\chi$ simulations for three different values of the SNR of the target and the template.
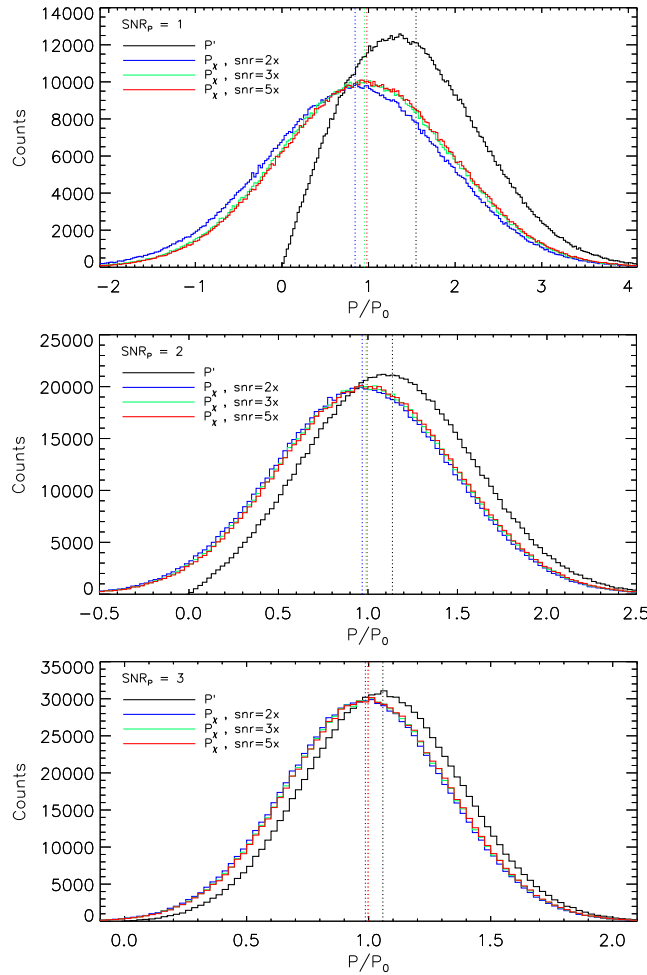
Figure 5. Histograms showing the distribution of $\hat{p}_\chi$ (coloured lines) and the naive (black line) estimator for three values of SNR in the target (top to bottom) and three values of the SNR of the template (as a multiple of the SNR of the target). All histograms are for the isotropic case, $\sigma_Q = \sigma_U$.

4.2 General case

Here we allow for asymmetric errors in Q, U, i.e. for $r < 1$. We created a grid of 100×100 different values of Q_0/σ_Q and U_0/σ_Q, in the range $Q_0/\sigma_Q \leq 4$, $U_0/\sigma_Q \leq 4$, using a uniform spacing. This was repeated for four values of r. We set $\theta = 0$, so that $r = \sigma_U/\sigma_Q$ (the pattern in the (Q, U) plane simply rotates for other values of θ). Then, $\times 10^5$ Gaussian noise realizations are added to the each point in the grid. We calculated the 'observed' polarization amplitude P' from the noisy simulations, applied the four estimators to each simulation, and in each case measured the mean bias $b = (\langle \hat{p} \rangle - P_0)$ for each pixel. The first column of Fig. 6 shows the bias of the naive estimator P'. The second column shows the residual bias after using the MAS estimator. The biased regions in the SNR plane reduces considerably in comparison with the first column that has no correction. The third and fourth columns shows the residual bias using the known-angle estimator. As this estimator requires an independent value for the polarization angle along with the observed values (Q', U'), we generated an additional $\times 10^5$ Gaussian realizations for the Q, U Stokes parameters of the template and with them, we reconstructed the known polarization angle, centred at the true value, χ_0, for each SNR value. Here, the SNR of the template is 2 (third column) and 3 (fourth column) times the SNR of the target.

As expected, apart from numerical noise, these results agree with the exact calculation shown in Fig. 3.

4.3 WMAP simulations

WMAP provided maps at five frequency bands between 23 and 94 GHz (Bennett et al. 2013). In the lower three frequencies, the sky polarization is dominated by Galactic synchrotron emission, with a brightness temperature that drops steeply with frequency ($T_\nu \propto \nu^\beta$, with $\beta \approx -3$). Since the brightness temperature sensitivity is similar in all bands, the highest SNR is at 23 GHz (*K* band), where large areas of diffuse polarized emission have SNR > 3 after smoothing to $1°$ full width at half-maximum (FWHM) resolution. In these bands, the synchrotron polarization angle reflects the Galactic magnetic field direction in the source regions, and is expected to be almost independent of frequency. The most likely cause of any frequency variation is superposition on the line of sight of regions with different field directions and also difference spectral indices β; however, the variation of β for the synchrotron component is small as has been shown by Fuskeland et al. (2014) and (Vidal et al. 2015). On the other hand, the higher *WMAP* bands begin to be sensitive to dust polarization, which has $\beta \approx +1.7$, and
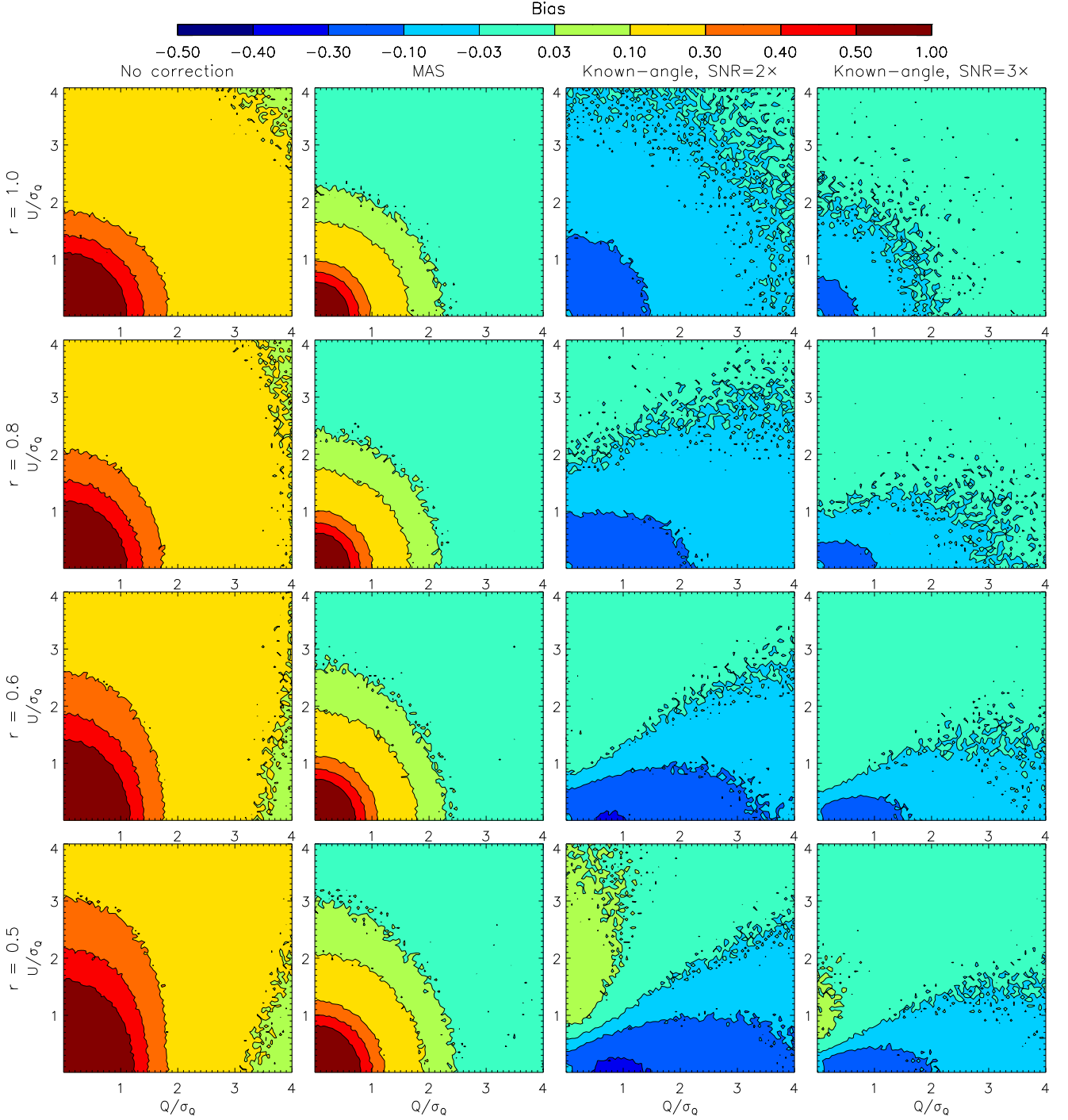
Figure 6. Contours of the mean residual bias of three estimators for the polarized intensity as a function of (Q, U), calculated using Monte Carlo simulations for four different values of the error ellipse axial ratio, r. We take $cov_{QU} = 0$ (there is no loss of generality, as the covariance can always be eliminated by a rotation of the $Q - U$ axes). The colour scale represents the percentage bias of the estimated polarization value in each pixel. The left column shows the naive estimator, $\hat{p}'$. The second column shows the MAS estimator, $\hat{p}_{MAS}$, from Plaszczynski et al. (2014). The third and fourth columns show the known-angle estimator, $\hat{p}_\chi$, presented in equation (22) for two different SNR levels of the angle template: 2 times and 3 times the SNR of the target.

Planck data confirm that this is generally significantly misaligned with synchrotron (Planck Collaboration XIX 2015a; Planck Collaboration XXII 2015b). For this reason, we only consider the three lowest *WMAP* bands below.

Fig. 7 show histograms of the SNR for the Stokes parameters (Q, U) of the three frequency bands: K (23 GHz), Ka (33 GHz) and Q (41 GHz) bands. The polarization SNR in K band is larger than the SNR in the other bands for almost the entire sky; in fact, the SNR in the Ka, and Q bands rarely exceeds 3. In Fig. 8, we show histograms of the axial ratio of the error ellipses for all the pixels in these *WMAP* bands. The mean ratio for all the bands is $r = 0.86$.
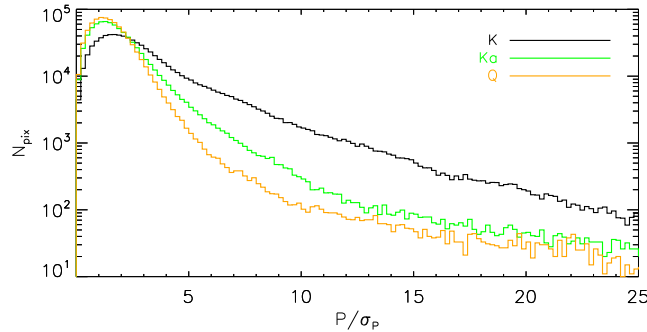
Figure 7. Histograms of the estimated signal-to-noise ratio of the polarization amplitude, $\mathrm{SNR_P} = P/\sigma_P$ of *WMAP* data in three frequency bands. The histograms are made using the full-sky maps at an angular resolution of $1°$, with $N_{\mathrm{side}} = 256$. The percentage of pixels where the SNR at *K* band is larger than the SNR at *Ka* and *Q* bands is 75 per cent and 78 per cent, respectively.
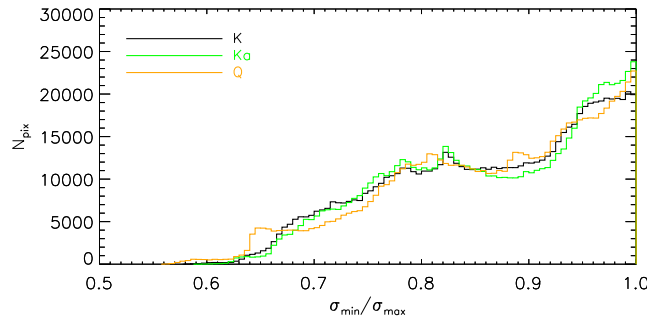
Figure 8. Histograms of the polarization error ellipse axial ratio (equation 13) of *WMAP* data in three frequency bands. The histograms are made using the full-sky maps at an angular resolution of $1°$, with $N_{\mathrm{side}} = 256$.

We used the *Planck* Sky Model (PSM; Delabrouille et al. 2013) to simulate the polarized sky at *K*, *Ka* and *Q* bands at an angular resolution of $1°$, from which we can obtain maps for the unbiased polarization amplitude, P_0. The model is closely based on the *WMAP K*-band map, and uses realistic spectral indices. We added random noise, generated using the *WMAP* covariance matrices C for each pixel, to the simulated Stokes Q and U map. The maps are generated at HEALPIX $N_{\mathrm{side}} = 512$. Smoothing was done by transforming to spherical harmonics, which were then divided by the *WMAP* instrumental window functions and multiplied by the window function of a Gaussian beam with $1°$ FWHM, then re-transformed. Noise and sky model maps were downgraded to $N_{\mathrm{side}} = 64$ to give approximately independent pixels, and summed to give maps of the 'observed' polarization amplitude, P'. In the top panel of Fig. 9, we show the reconstructed simulated polarization angle map at *K* band. The middle and lower panel of Fig. 9 show the observed polarization angle by *WMAP* at *Ka* and *Q* bands, respectively. We can see that the simulated *K*-band angles, which we use as our template is very similar (but less noisy than) the observed angle at *Ka* and *Q* band. This is the characteristic that the known-angle estimator requires.

We corrected for the bias in these P' maps using the same three estimators discussed in Section 4.2. *Ka* and *Q* bands are corrected using the known-angle estimator where the angle information required by the $\hat{p}_\chi$ estimator is measured from the *K*-band map. We then compared these de-biased maps with the true polarization amplitude map from the PSM simulations. In Table 1, we list the normalized bias value, averaged over the entire sky of 500 simulations for the three frequency bands that we studied.

The mean uncorrected bias, $\langle \Delta \hat{p}' \rangle = \langle P' - P_0 \rangle$ increases with frequency due to the decrease in SNR. $\hat{p}_{\mathrm{MAS}}$ substantially reduce the bias at *K* and *Ka* bands, but *Q* band is so noisy that its impact is relatively modest. A clearer view of the effect of the estimators is revealed in the histograms of normalized errors, $P' - P_0/\langle \sigma_P \rangle$, shown in Fig. 10. In *Ka* and *Q* band, the histograms of the uncorrected polarization maps are not centred at zero (the three plots in the left-hand column). Where available, i.e. for *Ka* and *Q* bands, the $\hat{p}_\chi$ estimator performs dramatically better than $\hat{p}_{\mathrm{MAS}}$. Note also that the histograms of the $\hat{p}_\chi$ estimator have a clear Gaussian shape. This shows that the uncertainty on the estimator (equation 23) can be used safely.

In order to see where the residual bias is more important, we show maps of the fractional bias after the correction using the different estimators. Fig. 11 shows the fractional bias at *K*, *Ka* and *Q* band, for each of our estimators. Pixels where the residual bias is larger than 20 per cent are shown in grey. The $\hat{p}_{\mathrm{MAS}}$ estimator (second row) leaves a small residual bias over most of the sky (green areas in the figure). The $\hat{p}_\chi$ estimator (bottom row) performs clearly better. In Table 2, we list the percentage of the area of the sky with a residual fractional bias smaller than ± 0.2.

The excellent performance of the known-angle estimator in this case is due to the use of some extra information. The improvement is spectacular due to the very low SNR over much of the sky at the target frequencies. One could attempt to restore the signal to noise by simply smoothing to lower resolution, but this will fail when there is substantial real variation in the polarization angle, which would cause the Q and U signals averaged over large areas to tend towards zero. The great advantage of the known-angle estimator is that we correctly preserve
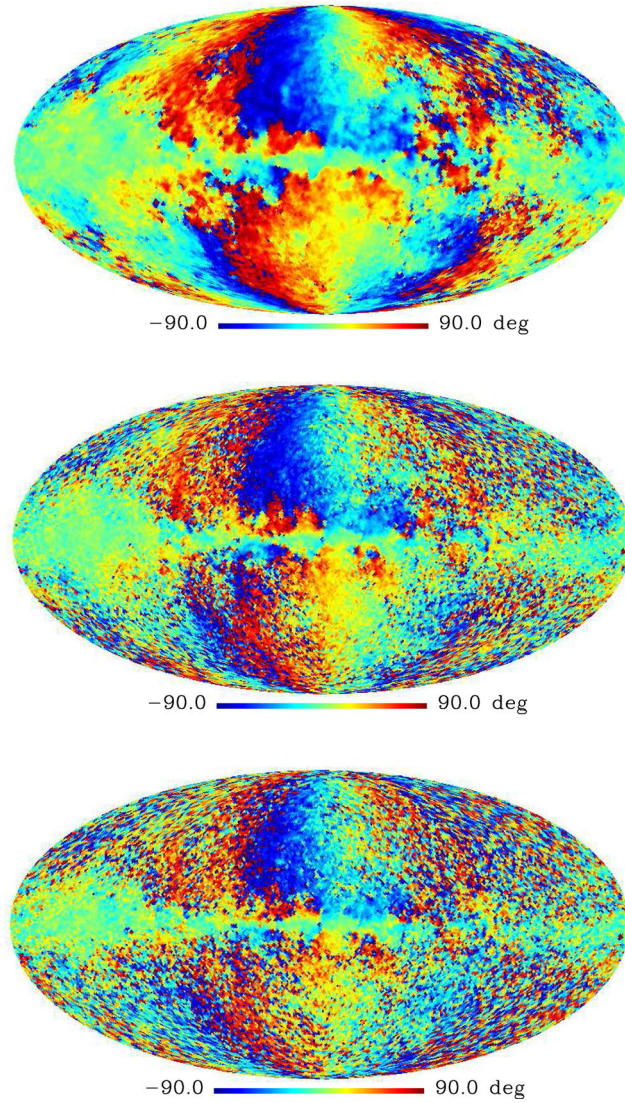
Figure 9. Full-sky polarization angle map. On top is the reconstructed angle map from the *Planck* Sky model with the added noise from *WMAP K*-band data. The middle and bottom panels show the observed polarization angle from *WMAP Ka* and *Q* bands, respectively.

Table 1. Full-sky averaged values for the normalized polarization bias and standard deviation of each estimator in simulated *WMAP* data, over 500 simulations. See Fig. 10 for the histograms of the errors $\hat{p} - P_0$.

Estimator	K-band		Ka-band		Q-band	
	$\langle\Delta\hat{p}\rangle^a$	std$[\Delta\hat{p}]^b$	$\langle\Delta\hat{p}\rangle^a$	std$[\Delta\hat{p}]^b$	$\langle\Delta\hat{p}\rangle^a$	std$[\Delta\hat{p}]^b$
$\Delta\hat{p}'$	0.20	0.98	0.50	0.91	0.66	0.87
$\Delta\hat{p}_{MAS}$	0.06	1.00	0.27	0.93	0.42	0.88
$\Delta\hat{p}_\chi$	–	–	−0.05	1.01	−0.03	1.01

*Notes.* ^{a}mean normalized bias, $\langle\hat{p} - P_0\rangle/\langle\sigma_P\rangle$ where σ_P is given by equation (17).
^{b}Standard deviation of $\hat{p} - P_0$, again in units of the mean error.

the true polarization direction while still allowing coherent averaging of the polarized amplitude. Vidal et al. (2015) uses $\hat{p}_\chi$ to measure the spectral index of the diffuse synchrotron polarized emission over large regions of the sky, an ideal application of the known-angle estimator. It can also be applied in the *Planck* data, both for the low-frequency synchrotron emission and also for the high-frequency dust polarization, where a natural template would be the highest available frequency, since the dust emission rises with frequency (Planck Collaboration XXII 2015b).
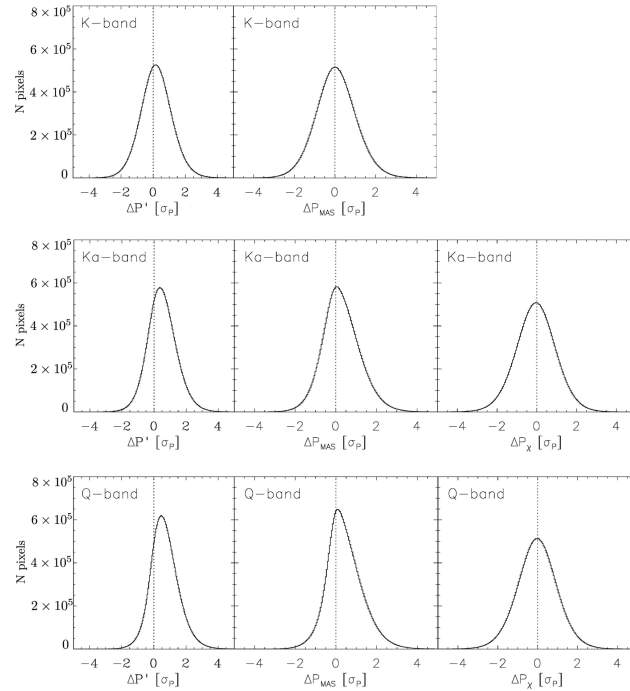
Figure 10. Histograms showing the bias of the three estimators studied for the simulated *WMAP* data at K, Ka and Q band described in the text. Histograms combine all 500 simulations and all sky pixels. They show the distribution of the difference between the estimators and the true polarization amplitude P_0, in units of the average polarization noise, $\langle\sigma_P\rangle$. The column on the left shows the histograms of the polarization bias of the naive estimator, i.e. the $\Delta P_0 = P'$ $- P_0$ (no bias correction). The second column shows the residual bias for the MAS estimator, $\Delta P_{MAS} = \hat{p}_{MAS} - P_0$. For the noisier bands (Ka and Q), the histograms are not centred at zero, implying that there is additional residual bias on the corrected map. The third column shows the histograms produced using the $\hat{p}_\chi$ estimator, $\Delta P_\chi = \hat{p}_\chi - P_0$. Here the bias correction works much better and the distributions for the three bands are centred at zero. Table 1 lists the central values and spreads for all these histograms.
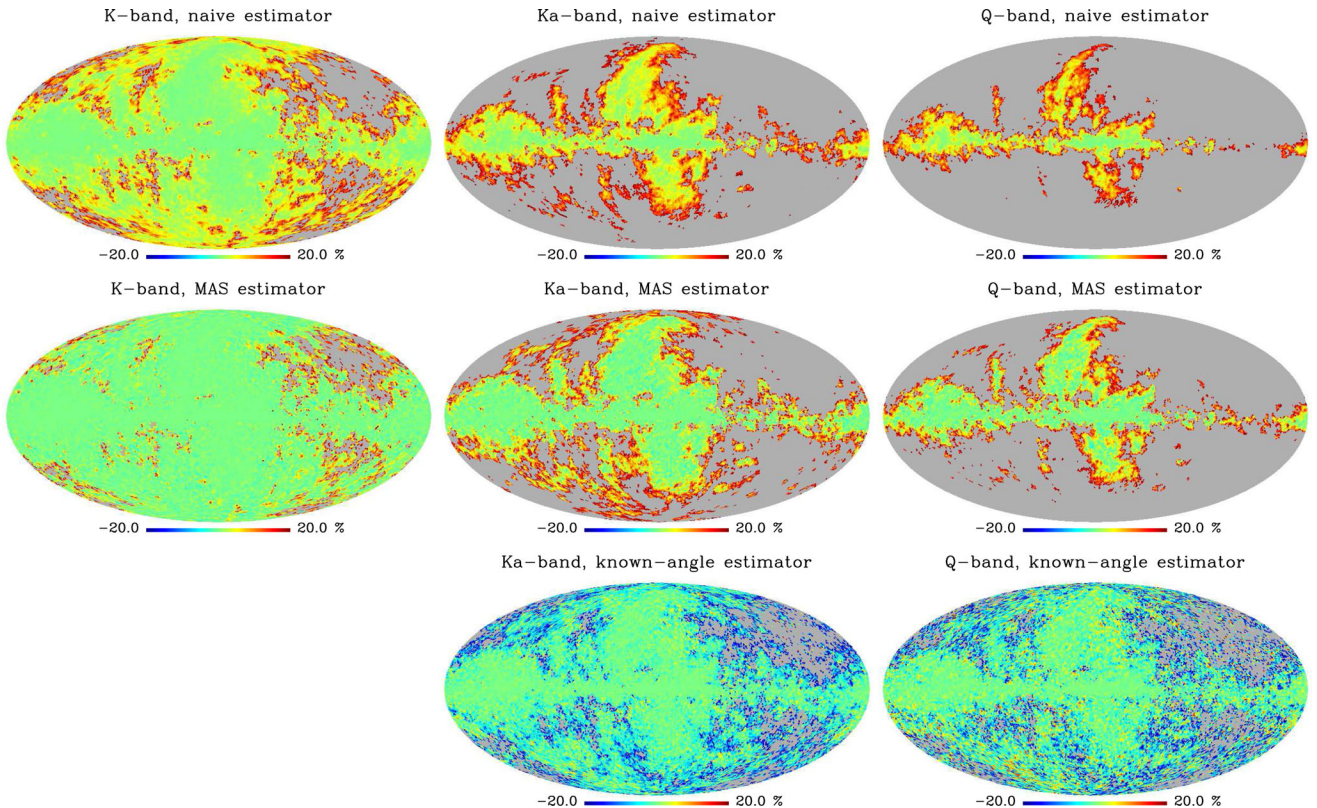
Figure 11. Maps showing the fractional bias in the *WMAP* K, Ka and Q bands (left-hand, middle and right-hand columns, respectively). The top row shows the fractional bias for the naive estimator $P' = \sqrt{Q'^2 + U'^2}$. The second row shows the residual bias when using the $\hat{p}_{MAS}$ estimator and the bottom row has the residual bias that remains after correcting with the $\hat{p}_\chi$ estimator. All the pixels with an absolute value larger than 0.2 are shown in grey.

Table 2. Percentage of the area of the full-sky map that have an absolute value of the residual fractional bias smaller than 0.2. These areas corresponds to the coloured pixels in Fig. 11.

Estimator	K-band per cent	Ka-band per cent	Q-band per cent
P'	84.9	35.0	18.4
$\hat{p}_{\text{MAS}}$	91.5	53.3	29.5
$\hat{p}_{\chi}$	–	84.8	84.3

5 CONCLUSIONS

We have proposed a new way of correcting for the positive bias that affects the polarization amplitude. The 'known-angle estimator', $\hat{p}_{\chi}$, works when there is independent and high SNR information about the polarization angle of the observed source. This additional information helps to reduce the polarization amplitude bias.

We have derived formulae for the estimator, its precision, and its residual bias, due to the uncertainty in the template angle that is used. The estimator is continuous, analytic, possibly negative and highly Gaussian. Given an independent good template for the polarization angle, i.e. the SNR of the template is at least 2 times the SNR of the target, this estimator performs excellently in the low SNR regime. We have shown with simulations using *WMAP* data that the known-angle estimator, $\hat{p}_{\chi}$, outperforms the MAS estimators, which is not surprising as $\hat{p}_{\chi}$ uses additional information about the U/Q ratio to correct for the bias. We believe that this new estimator will be of great use in data sets that encompass multiple frequencies with different SNR rations like *Planck*, or even in multiwavelength analysis mixing optical, infrared and radio data.

REFERENCES

Bennett C. L. et al., 2013, ApJS, 208, 20
Delabrouille J. et al., 2013, A&A, 553, A96
Fuskeland U., Wehus I. K., Eriksen H. K., Næss S. K., 2014, ApJ, 790, 104
Górski K. M., Hivon E., Banday A. J., Wandelt B. D., Hansen F. K., Reinecke M., Bartelmann M., 2005, ApJ, 622, 759
Kendal M., Stuart A., Ord J. K., 1994, Kendall's Advanced Theory of Statistics. Vol. 1: Distribution Theory. Willey, UK
Montier L., Plaszczynski S., Levrier F., Tristram M., Alina D., Ristorcelli I., Bernard J.-P., 2015a, A&A, 574, A135
Montier L., Plaszczynski S., Levrier F., Tristram M., Alina D., Ristorcelli I., Bernard J.-P., Guillet V., 2015b, A&A, 574, A136
Planck Collaboration I, 2014, A&A, 571, A1
Planck Collaboration XIX, 2015a, A&A, 576, A104
Planck Collaboration XXII, 2015b, A&A, 576, A107
Plaszczynski S., Montier L., Levrier F., Tristram M., 2014, MNRAS, 439, 4048
Quinn J. L., 2012, A&A, 538, A65
Rice S. O., 1945, Bell Syst. Tech. J., 24, 46
Serkowski K., 1958, Acta Astron., 8, 135
Simmons J. F. L., Stewart B. G., 1985, A&A, 142, 100
Vaillancourt J. E., 2006, PASP, 118, 1340
Vidal M., Dickinson C., Davies R. D., Leahy J. P., 2015, MNRAS, 452, 656
Vinokur M., 1965, Ann. Astrophys., 28, 412
Wardle J. F. C., Kronberg P. P., 1974, ApJ, 194, 249

This paper has been typeset from a TEX/LATEX file prepared by the author.